Hindawi
Advances in Civil Engineering
Volume 2022, Article ID 7874066, 19 pages
https://doi.org/10.1155/2022/7874066

Research Article

A Study on Self-Consolidate Concrete in Experimental Reinforced-Concrete Beam Column Structures with Alccofine and Steel Fiber

G. Vimal Arokiaraj and G. Elangovan

Department of Civil Engineering, University College of Engineering, Thirukkuvalai, Nagapattinam, Tamil Nadu, India

Correspondence should be addressed to G. Vimal Arokiaraj; gvvimal@gmail.com

Received 21 July 2022; Accepted 6 October 2022; Published 31 October 2022

Academic Editor: Eleftherios K. Anastasiou

This paper discusses the concept of self-consolidating concrete mix with Alccofine-1203, superplasticizer, viscosity modification agent, crimped steel fiber on the RC beam column joint. Totally, eight reinforced-concrete (RC) column joints with M25 grade concrete were considered in this study. Out of eight RC beam column joints, two beam column joints served as Alccofine, two beam column joint specimens served as Alccofine 5%, two beam column joint specimens served as Alccofine-10%, and two beam column joint specimens served as Alccofine-15%. All the RC beam column joint specimens were tested under the compression until failure in the loading frame of 2000 kN capacity. The test results of Alccofine-10% showed the higher loading capacity than that of Alccofine-5% and Alccofine-15% in self-consolidating concrete RC beam column joints. The percentage of superplasticizer, viscosity modification agent, and crimped steel fiber is maintained. Nonlinear finite element analysis (FEA) to analyse the beam column joint through nonlinear finite element modelling (NLFEM) and the modelling results were compared from the experimental results. The results obtained through ANSYS modelling show good agreement with the experimented results. The deflection ductility of experimental results shows 1.57, and the predicted deflection ductility shows 1.59 in beam column joint with Alccofine-10%. ANSYS software is validated as appropriate software to predict the study parameters of self-consolidation concrete in beam column joints.

1. Introduction

Self-compacting concrete/self-consolidating concrete (SCC) in ASTM subcommittee (C09.47) is a type of concrete that is self-compacting described as concrete without compaction or vibration conditions. As the name implies, SCC avoids water while decreasing its volume by self-compaction without any external energy. Consequently, it is often called self-consolidation. In 1986, Professor Hajime Okamura of KCT, Japan, conceived the concept as a response to the Japanese administration's increasing concerns regarding longevity. Through his work, Okamura discovered that the key cause of Japanese concrete's low durability efficiency in structures was insufficient concrete consolidation in the casting operation. The design was developed by 1988 and primed for the first real-scale experiments. SCC refers to concrete that self-consolidates on its own weight without the use of vibration that has been used in the construction sector for years. We obtained fluidity by adding gas, superplasticizer, or a mixture of both. Furthermore, the earlier form of concrete is not used in civil engineering structures with standard criteria for longevity because they either produced too much water or were not durable and resulting in undesirable structural heterogeneity.

With its adjusted pore size distribution, Alccofine has unique properties that improve the efficiency of concrete in both the strength and durability stages. Alccofine is a suitable solution for silicate because it has an ideal distribution of particle size that is neither excessively fine nor too coarse. Alccofine is manufactured under specific restrictions using specialized equipment and devices to generate an optimum distribution of particle size, being its

distinguishing feature. The beginning hardness of Alccofine-1203 concrete is similar to or higher than that of silica because it initiates the fundamental process after hydrating, and Alccofine also absorbs by-product hydroxide ions from production of cement from added C-S-H gel that is comparable to pozzolana. Based on the material size distribution, the calculated selection of the participants number is roughly 1200 cm^2/gm, which is genuinely nanoscale. It improved the decrease of cementitious and enlarged slump retention without growing the contaminant intermixing dosage, as well as being quick and efficient, it forced to close removal, fast form line up in the prefabricated concrete industry, and improved the percentage of resilience acquired in concrete mixtures with pozzolanic material resource components such as fly ash, GGBS, and others. In addition to concretes and other pozzolanic powder ingredients, the approximate of Alccofine-1203 should be added the mixture mix. The mixing ratio must be long enough to allow for homogeneous intermixing of all powder ingredients in the concrete. Dose ranges from 4% to 8% by mass of the total binder material, depending on the grade of concrete.

India has already been illustrious to be an associate earthquake prone space. Here, most residential buildings are reinforced-concrete (RC) structures. Beam column joints are basic components of pillars that contact with beams near their intersection in strengthened concrete structures. Because the joints' chemical compositions have limited durability, they can only carry a limited amount of force. Joints are heavily affected when stresses greater than this are applied during disasters. The bulk of the structures that are still being constructed using indigenous techniques do not follow the codal provisions because of lack of data and steering. Such nondesigned constructions area unit principally rife in earthquake prone areas of the developing world that embrace countries like India, Pakistan, Turkey and Iran. In Indian structural style practice, the beam column joint is usually neglected for a specific style. As per the present codes, the concentration is proscribed solely to providing comfortable anchorage for the longitudinal reinforcement of the beam reinforcement within the columns. Because of this negligence, there are so many requirements of jacketing and retrofitting at the junction and joints. The destructive effects of joints on the cyclic behaviour of RC buildings (especially framed ones) prompted advances in the contemporary RC structure structural hazard. As a result, the capacities design method was launched in the middle of the 1960s–1970s, which has been founded on the controlled and hierarchical structure organized damage limitation philosophy. As a result, the development of new protocols for the design of beam-column connections in structural systems attempts to create joints that will remain untouched throughout cycle, while destruction and the production of plastic hinges is anticipated in the neighbouring beam. Various geological code requirements harmonized after a study of experimental investigations discovered in the research take into account the variety of beam-column junction configurations.

Nonetheless, evidence collected during the evaluation of nicely built joints is in accordance with the current standards and is insufficient to fully substantiate code restrictions. For example, the normal systems of Euro code 8 (EC8) relating flexibility classifications moderate (DCM) structures for the construction of multistorey building frames which provide no guidelines for estimating joint shear strength. Joint shear forces (both horizontal and vertical) are, nevertheless, substantially greater than those resisted by the building elements framing the joint (i.e., beams and columns). As a result, the vast majority of current European architectural features to EC8 (DCM) are vulnerable to early fragile shearing damage or collapses during future significant earthquakes, which could result in the partial or whole collapse. Furthermore, practicing civil engineers are completely uninformed of the true magnitude of the forces acting and are resisted by the beam-column junctions of RC structures planned so according to EC8 during the design process (DCM).

The ductility index of the reinforced-concrete element has been the subject of many research objectives and critical analysis recently, and scare consideration is carried out to measure the ductility of reinforced self-compacting concrete (SCC) enhanced with steel fiber. Hence, to evaluate the ductility, in terms of energy absorption, of reinforced steel fibrous self-compacting concrete beams subjected to experimental flexural force, totally, twelve-reinforced SCC beams experimented under flexural loads including pair groups of six beams with and without steel fibers, minimum and maximum steel ratio, and three grades of concrete G20, G50, and G60 are used. The results also reveal that the increase of fibrous material to SCC is extremely efficient and also increasing energy dissipation, flexural capacity, and ductility index. Besides, the flexural strength grows with increasing steel fiber percentage, steel reinforcement ratio, and concrete compressive strength [1]. The response of the structure under the earthquake loads mainly depends on the behaviour and performance of the beam column joint (BCJ). An experimental investigation on exterior reinforced beam column joints done using steel fiber reinforced self-compacting concrete subjected to reversed cyclic loading is presented in this investigation. The attempt has been made to demonstrate the influence of steel fibers reinforced self-compacting concrete (SCC). The results show enhanced ductility, energy dissipation capacity, and damage tolerance behaviour with the increase in steel fibers percentage in SCC [2]. Analysis of beam column joints prepared using self-compacting concrete (SCC) is incorporated with nanosilica (NS) and recycled coarse aggregates (RCA). For this purpose, the beam column joint behaviour of normal concrete and SCC incorporating RCA and NS were examined under static loading condition [3]. The reinforced-concrete structures, glass fiber reinforced polymer (GFRP) rebars can be an appropriate substitution to steel rebars for emphasizing concrete buildings in worse environments. The flexural behaviour of reinforced Alccofine-based SCC beams with steel and GFRP rebars has not yet been attempted before. The influence of reinforcement and SCC mix proportions on the load-bearing capacity, deflection, cracks, strains of concrete, and reinforcement and moment were examined. From this findings, it was determined that beams reinforced with steel failed under flexure whereas GFRP

caused the brittle failure [4]. Experimental and analytical work is carried out to investigate the behaviour of GFRP reinforcement versus traditional steel reinforcement in self-compacting concrete columns under eccentric loads. The GFRP-reinforced columns have lower carrying capacities than the steel-reinforced columns, with a difference of 24%. The analytical results show good agreement with the experimental results for steel-reinforced columns [5]. Self-compacting concrete is one of the best solutions to solve the structural problems at the joints. In this investigation, M25 and M40 grade self-compacting concrete properties are analysed by comparing with the conventional concrete. These specimens are tested on the loading frame to analyse the carking pattern, load carrying capacity, and maximum deflection produced at the joints [6].

Nonlinear finite element analysis (FEA) of RC beam column connections is performed in order to investigate the joint shear failure mode in terms of joint shear capacity, deformations, and cracking pattern. The comparison between experimental and numerical results indicates that the FE model is able to simulate the performance of the beam column connections and is able to capture the joint shear failure in RC beam column connections [7]. To investigate and analyse the fracture parameters, the SEM (size effect method) and WFM (work fracture method) were used. Results have shown that in both methods, an increase in percent steel fibers increases the fracture energy and makes the concrete more ductile, but in WFM, the results are more specified because it considers the postpeak. Results show that fibers can, in some cases, reduce the size effect [8]. Analyses on the seismic performance of exterior beam column joints strengthened with the unconventional reinforcement detailing. The beam column joint specimens were tested with reverse cyclic loading applied at the beam end. The experimental studies are proven with the analytical studies carried out by finite element models using ANSYS. The results show that the hysteresis simulation is satisfactory for both unstrengthened and ferrocement strengthened specimens [9]. The variables include the type of beam longitudinal bar anchorage in the joint, the transverse reinforcement of joint, and the strength of concrete. Experimental and analytical investigation of joint behaviour is carried out. In the experimental part, 10 semiscale exterior beam column joints were manufactured and subjected to a constant column axial load and beam quasi-static cyclic load. In the analytical part, the ABAQUS software is used for modelling and analysing of test specimens. Based on the results, the experimental and analytical joint capacities are in good agreement. Results show that using self-consolidating concrete in joints, apart from easier concrete placement, can increase the workability and ductility of connection and result in a better bond with reinforcing bars [10], tested under reversed cyclic loading applied at the beam tip and at a constant axial load applied on the column. The beam column joint specimens were instrumented with linear variable displacement transducers and strain gauges to determine load displacement traces, cumulative dissipated energy, and secant stiffness [11]. The proposed model provides a simple representation of the primary inelastic mechanisms that determine joint behaviour. The failure of the joint core under shear loading and the anchorage failure of beam and column longitudinal reinforcement are embedded in the joint. The comparison of simulated and observed response for a series of joint subassemblages with different design details indicates that the proposed model is appropriate for use in the simulating response under earthquake loading [12]. A commercially reproducible high-strength self-compacting concrete, a conventionally vibrated high-strength concrete, and a normal strength conventionally vibrated concrete were designed. Totally, seven beam column joints were designed. All BCJs were tested under a displacement-controlled quasi-static reversed cyclic loading. The load, displacement, drift, ductility, joint shear deformations, and elongation of the plastic hinge zone were also measured during the experiment. It was observed that not only none of the seismically important features were compromised by using HSSCC but also the quality of material and ease of construction boosted the performance of the BCJs [13]. Totally, ten self-compacting concrete specimens were tested, under static and cyclic loading. These consist of a set of one control SCC and four strengthened SSC specimens of different percentages of fiber for static loading and similarly another set for cyclic loading. Experiments were carried out to observe the optimum dosage and influence of hybrid fiber on self-compacting concrete beam specimens in static and cyclic loading. Evaluate load carrying capacity, energy dissipation, and the initial stiffness improvement of hybrid fiber reinforced self-compacting concrete beams with respect to the control self-compacting concrete beam specimen under both static and cyclic loading. It can be concluded that the incorporation of hybrid fiber with optimum dosage in concrete improved the the ductility of concrete, and failure was more ductile compared with control specimens [14]. The results show an experimental program carried to explore the possibility of fly ash and Alccofine as partial replacement of cement in self-compacting concrete. SCC mixes were designed and cement was replaced with fly ash 25% and Alccofine-5, 10, and 15% respectively. Results indicated that compressive, split tensile strength and the modulus of rupture of self-compacting concrete improved with the incorporation of 25% of fly ash and 10% of Alccofine at all the curing ages [15]. Four series of SCC mixes are prepared and different percentages of Alccofine were added from 0 to 60% with two varying W/B ratio of 0.35 and 0.4 and SP dosage of 1% and 1.5%, respectively. The fresh properties are determined as per directions of the EFNARC. The compressive strength is reported at the age of 7 and 28 days and compared with the conventional SCC. From the findings, the SCCA30 mixture showed better performance in all the series, and series-3 is chosen for the finer performance to satisfy both fresh and hardened properties of SCC [16]. Totally, seven mixes were prepared with different percentages of Alccofine 4–14%. The concrete mixes were experimentally tested for compressive, flexural, and split tensile strengths for 7, 28, and 56 days. Uniaxial stress-strain behaviour, water absorption, and porosity were evaluated at the 28-day curing period. Young's modulus, energy absorption capacity (EAC), and integral absolute error (IAE)

were assessed analytically. From the test results, mixing with 10% Alccofine content exhibited good behaviour in all the investigated parameters. The Alccofine incorporation was found to have a negative effect on the behaviour of HSC beyond 10% replacement in all the investigated parameters [17].

2. Material Properties

The cement considered in this investigation is Ordinary Portland Cement (OPC) 53, and standard grades were used in compliance with IS: 12269-1987. Fine aggregate used during the investigation was nearby obtainable river sand confirming to zone II based on IS 383-1970. Alccofine-1203 is a substance made from high reactivity glass, obtained via the controlled granulation cycle. The raw materials are mainly made of silicates poor in calcium. Steel fiber is commonly used to improve concrete's tensile strength and ductility. Crimped steel fiber conforming to ASTM A820-01 is used in this research work since the bonding ability is greater than other steel fiber forms. The locally available coarse aggregate with the confirmation of code EFNARC for the effective utilization of coarse aggregate to prepare self-consolidated concrete is 10 mm. The size of the coarse aggregate influences the flow behaviour; hence, choosing the size also plays a major role to prepare self-consolidating concrete. A new modified polycarboxylic ether based superplasticizer Master Glenium SKY 8233 and Glenium Stream2 which is compatible viscosity modifying agent were used in this research. Portable water which is free from salt, acid, and organic substances is used for mixing and curing confirming to IS 456-2000.

3. Experimental Investigation

The M25 grade of self-consolidation concrete with the mix ratio of 1 : 2.45 : 1.78 : 0.36 : 0.02 was used in this study. Based on the preliminary experimental test results, the percentages of Alccofine, crimped steel fiber, superplasticizer, and viscosity modification agent were already optimized as per EFNARC guidelines. The experimental investigations are calculated as on eight beam column joints. The column has a size of 150 × 200 mm and 2000 mm height and beam has a size of 200 × 150 mm and 1000 mm length. All the beam column joints were provided with four bars of 12 mm diameter as longitudinal reinforcement and 8 mm diameter mild steel as ties, spaced at 150 mm·c/c. The description of the test results are presented in Table 1. The instrumentation for a typical beam column joint with reinforcement details and the experimental test setup are shown in Figures 1 and 2. Figure 3 show the various steps involved in preparation of testing specimens.

Out of the eight beam column joints, two served as control specimens without Alccofine, two beam column joint specimens with Alccofine 5%, two beam column joint specimens with Alccofine 10%, and two beam column joint specimens with Alccofine 15%. The RC beam column joints were verified on a loading frame of 2000 kN capacity. The RC beam column joints by applying monotonically increasing compressive load at increments of 2 kN and the actual test setup on beam column joint under axial compression and flexure are shown in Figure 4. The specimen was placed on the loading frame and LVDTs are used to evaluate beam deflections just at the transition point and semijoints. The deformation at the midpoint of the columns is measured with some other LVDTs. A hydraulic actuator (capacity 10 tonnes) was utilised to provide a downward direction force on the the upper side of the beam at a separation of 90 mm from of the beam and column interfaces, causing the joint to stretch and rip. 1 kN load increases were applied to the beam. During the loading, the LVDT values from the deformation indication are captured at periodic intervals. As flaws spread and evasions begin to rise rapidly, dial indicators are eliminated and the loading on the beams is raised until it fails, and whenever the force applied to the beam began to decrease, the sample was judged unsuccessful. There are additional findings made in relation fracture development and joint progressive collapse. The metal fracture patterns and specimens with Alccofine in SCC control with about 5%, 10% and 15% are shown in Figures 5–8.

4. Experimental Test Results and Discussion

The experimental results are taken for 8 RC beam column joint specimens to compute the effect of conventional and self-consolidating study parameters considered in this investigation which are loads, deflections, and stresses. Parameters like deflection, ductility, deflection, and ductility ratio are also studied in this investigation. The load deflection behaviour of the all tested specimens is shown in Figure 9. Results related to critical load, critical axial deflection, critical lateral deflection, critical stress, deflection ductility, and energy ductility of the tested specimens are presented in Table 2 and Figures 10–14.

5. Analysis and Design of Beam Column Joint

In resisting moment frames, beams and columns are connected at one point which is known as the joint of beam and column. In the RC column joint structures, beam column joints are critical zones for transferring loads efficiently concerning the joining elements like beams, slabs, and columns because the joints are assumed as rigid.

5.1. Analysis of a Five-Storey Building. To know the behaviour of joints, a five-storey reinforced-concrete building was taken for the analysis using STAAD Pro:

Size of the floor = 4.00 m × 4.00 m

Unit weight of concede = 25 kN/m^3

Floor finish = 1.00 kN/m

Weight of 230 thick partition wall = 12.00 km/m^2

Weight of 115 thick partition wall = 6.00 m·c/c

Span of column = 3.00 m·c/c

Based on the worst combination of load, the value for bending moment and shear and axial forces is taken in the beam

Table 1: Specimen details.

Sl. no.	Specimen designation	AF (%)	SF (%)	SP, VMA (agent)	Tensile strength of steel fiber
1	BCJ1-SCC1	0	0	0	1025
2	BCJ2-SCC2	0	4	0	1025
3	BCJ1-AL-SCC-5%	5	0	1.8	1025
4	BCJ2-AL-SCC-5%	5	4	1.8	1025
5	BCJ1-AL-SCC-10%	10	0	2.3	1025
6	BCJ2-AL-SCC-10%	10	4	2.3	1025
7	BCJ1-AL-SCC-15%	15	0	3.3	1025
8	BCJ2-AL-SCC-15%	15	4	3.3	1025

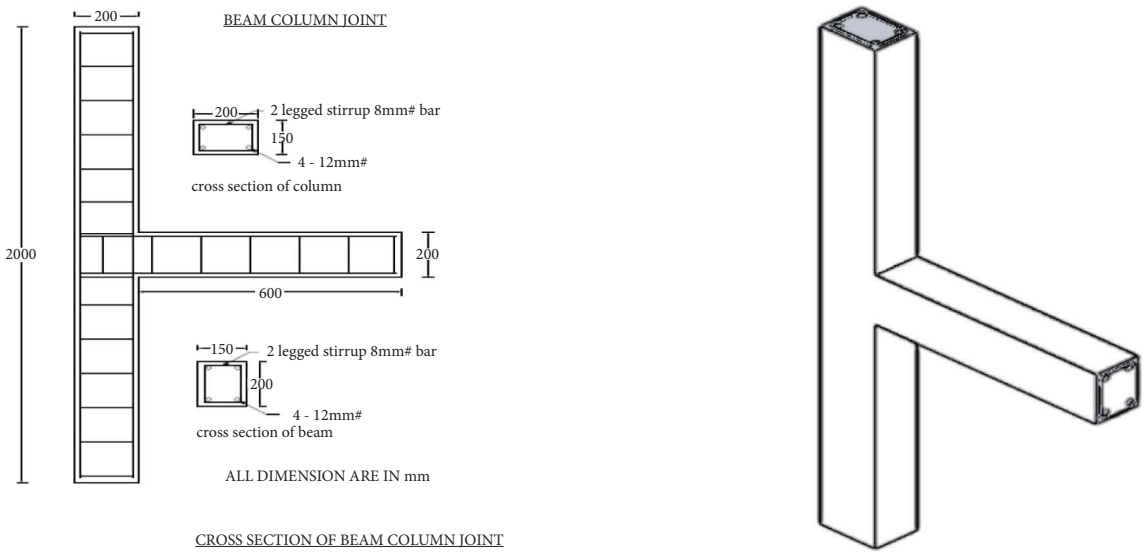

Figure 1: Typical beam column joint with reinforcement details.

column joint design. The bending moment profile for one load case is shown in Figures 15 and 16. The maximum bending moment occurred at the roof level of the ground floor. Design is carried out for the two beams (Beam No. 60 and 85) which have the maximum bending moment.

Simply supported beam Mu = wl2/8

Beam (1) Mu = 25.426 kNm, w = 12.10 kN

Beam (2) Mu = 25.156 kNm, w = 11.97 kN

Beam (77) Mu = 35.992 kNm, w = 17.12 kN

Axial load = 20.595 kN

Assume 1.5 times of axial load = Pu

Pu = 30.893 kN

5.2. Modelling of Hysteresis Curves Analytical. The hysteresis loop for the reinforced-concrete members, for evaluating the seismic behaviour of reinforced-concrete structures and the hysteretic behaviour of structural elements is critical. A mathematical model for the hysteresis loops of reinforced-concrete beam column connections is derived for beam column connection.

5.2.1. Hysteresis Curve. For evaluating the seismic behaviour of reinforced concrete, the hysteretic behaviour of structural elements is critical. It is difficult to idealise the analysis of reinforced-concrete components with a single model since there are so many aspects that influence it. As a result, it makes sense to utilise various models that are valid for particular range of the effective variables. A hysteretic framework for the medial load-deflection relation of reinforced-concrete components is presented for this goal, based on software data taken at the end of a research analysis using the ANSYS software, and these hysteresis loops are presented as parabola in terms of displacement level, column axial loads, and the number of inelastic cycles of displacement. During an earthquake, the ground moves in two horizontal directions as well as vertically in an intricate combination of frequencies and displacement. This ground movement causes a complex dynamic response of the multistorey structure. Numerical integration of the equations of motion of the structure which utilises the nonlinear structure member hysteresis loops can be used to predict the response of multistorey structure to earthquake. The accuracy of this integration procedure in predicting the response is limited by the accuracy of the individual structure member load displacement curves and the accelerogram record of the anticipated earthquake. The present equation for reinforcement concrete beam column connection hysteresis loops is derived based on the simulated earthquake conditions. The three parameters considered to be most important in describing this nonlinear behaviour are (1)

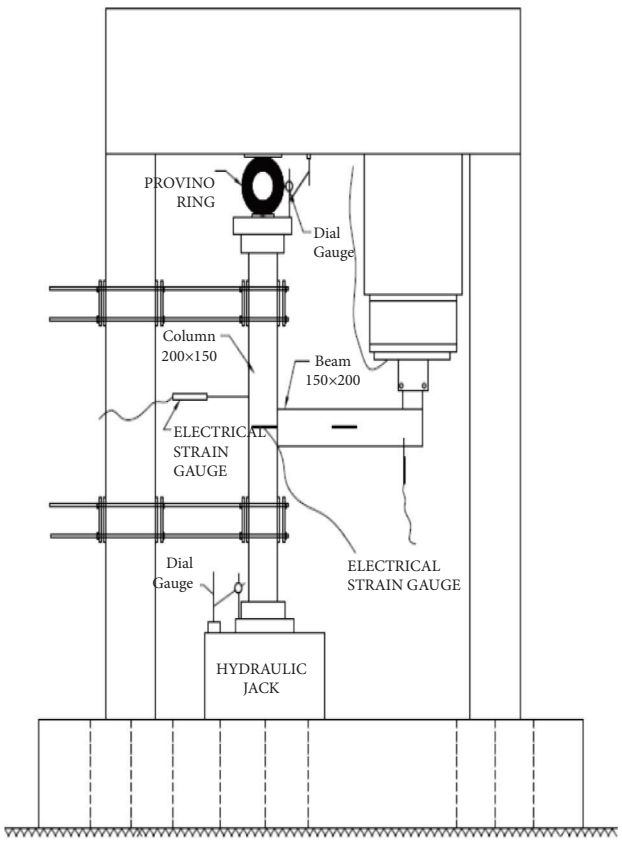

Figure 2: Experimental test set-up.

column axial load, (2) displacement level, and (3) the number of cycles of inelastic load.

5.2.2. Hysteresis Model for the Reinforced-Concrete Member. The characteristics are the slope of postpeak branch, and the slopes of unloading branches and level of pinching. The model is presented schematically as shown in Figure 17.

5.2.3. Postpeak Branch Slope. From the study, the experimental results show that the postpeak branch slope of the load displacement relationships can be represented by a single line that may either have positive or negative slope. While strength degradation is basically a function of achieved ductility level, the level of axial load also plays the vital part on the slope of the postpeak branch, consequently on the rate of strength degradation.

ΔP is the strength degradation, Pu is theoretically determined ultimate load, is the achieved displacement, and Δy is the displacement that corresponds to yielding:

$$\frac{\Delta P}{P_u} = 0.0107\,(5.219 - 80.332v)\,\frac{(\delta - \delta_y)}{\delta_y} + 0.0071. \quad (1)$$

Note that (1) may be valid for the members that have similar type of reinforcement. The slope of postpeak branch may significantly differ according to the strengthening characteristics of steel reinforcement.

5.2.4. Slope of the Unloading Branch. The geometric ratio of the longitudinal reinforcement is found to be effective on the slopes of the unloading branches, in addition to the initial stiffness and achieved displacement ductility ratio, as

$$\frac{k_{un}}{k_y}\,0.04520\left[(-46.03\rho - 0.025)\,\frac{\delta}{\delta_y} + 320.14\rho + 5.95\right] + 0.685, \quad (2)$$

where $k_{un}$is the slope of unloading branch at the displacement ductility level; $\delta/\delta y$ and ρ is the geometric ratio of longitudinal reinforcement to concrete section. k_y is determined by

$$k_y = \frac{p_u}{\delta_y}, \quad (3)$$

δy is the displacement at the theoretical ultimate load level, Pu, which is theoretically determined by using stiffness of cracked section.

5.2.5. Pinching. To establish pinching, a fictional interconnects of all of the other hysteretic on the load displacement long marriage initial rising branches are defined, and Pinter section and hysteresis loops increase by a decrease in the geometric ratio of longitudinal reinforcement and an increase in the level of axial load. The statistical evaluation of the relation between P intersection/Pu and ρv and v resulted in

$$\frac{p_{\text{intersection}}}{p_u} = 1.4\rho v^{-0.55} - 0.56v + 0.48. \quad (4)$$

5.3. Theoretical and Experimental Modelling of the Hysteresis Curve

5.3.1. Column Axial Load. In the study, the lateral forces produce overturning moments which increase the column stresses on the one hand of the structure, while reducing them on the other hand. This reduction in column stresses may occur during an instant of high vertical acceleration, which is ignored by most engineers, producing high column tensile loads. Goel, using a Ramberg–Osgood structural member model, found that overturning moment alone was great enough to cause column tension stresses equal to 2.5 times the gravity load stresses. Workman, using an elastoplastic model for a ten-storey frame, found that the total column tensile stress is as great as one-third of the yield stress of steel. There is little doubt that large tension loads can occur in columns during a large earthquake. This tension load is significant for reinforced concrete because concrete cracks at relatively low tensile stress requiring the entire tension load to be carried by the reinforcing steel. The resulting steel strains tend to open cracks in the connection reducing the stiffness and energy absorption of the connection. This effect of column tension, which has not been reported in the previous reinforced concrete research, is the first parameter investigated here.

(a) (b)

(c) (d)

Figure 3: Preparations of test specimen: (a) steel reinforcement cages, (b) wood flag and steel reinforcement cages, (c) casted specimen, and (d) white washing specimen.

5.3.2. Displacement Level. Displacement level, which is defined as the hinge rotation divided by that hinge rotation which would cause the top beam steel to yield, is the second parameter investigated. As loading is applied to the hinge, cracks formed in concrete before the reinforcing bars give yield. As loading increases, the cracks grow and new ones are formed, reducing the stiffness of the connection. When the load is reversed, these cracks close and new ones form. The opening and closing of cracks dissipates energy whether the steel yields or not. As the cracks open and close, particles are ground or crushed, further reducing the stiffness of the connection. The amount of stiffness reduction and energy dissipation is dependent upon the displacement level.

5.3.3. Cycles of the Inelastic Load. As the structure vibrates, the concrete is ground and crushed, changing the load displacement curves. Several researchers, who have tested model frames of reinforced concrete loaded beyond the yield point of steel (3), report rapid changes in stiffness during the first several inelastic cycles. The number of cycles of inelastic deformation is the third parameter considered in this research.

5.3.4. Hysteresis Loops. The equations derived from the analysis of these experimental hysteresis loops are converted to dimensionless variables for simplicity of presentation and utilization. The load coordinate for the hysteresis loops, is shown in Figure 18, as M/my, where M is the moment and

Figure 4: Actual test set-up on beam column joint under axial compression and flexure.

My is the computed moment which tensions the top steel to the design yield stress. Column axial load, σ, is the dimensionless ratio σ_T/f_c, and here f_c' is the design compression strength of concrete and σ_T is the axial stress on the transformed column strength. Displacement level, γ, is defined as $\varnothing/\varnothing_y$, where $\varnothing_y$ is the beam rotation ten inches (25.4 cm) from the column face caused by the moment M_y. The derived hysteresis loop equations are presented as four parabolas:

$$\frac{M}{M_Y} = a_i + b_i\gamma + c_i\gamma^2, \tag{5}$$

where

$$a_1 = 0.461 - 0.319log_{10}\rho + 0.0060\,\gamma_m - 0.671\sigma\,(\gamma > 0) \tag{6}$$

$$a_2 = 0.388 + 0.343log_{10}\rho - 0.015\gamma_m + 0.548\sigma\,(\gamma < 0) \tag{7}$$

$$b_1 = 0.685 - 0.125\gamma_m + 0.00591\gamma_m^2 \tag{8}$$

$$c_2 = 0.029 + 0.00764log_{10}\rho - 0.00209\gamma_m - 0.0127\sigma \tag{9}$$

$$c_3 = 0.03628 - 0.01625log_{10}\rho - 0.00242\gamma_m - 0.00283\sigma \tag{10}$$

$$c_4 = 0.00090 - 0.00284log_{10}\rho - 0.00011\gamma_m + 0.01634\sigma \tag{11}$$

Provided that,

$$\gamma_m \le 12.7\ and\ 0.25 \le \rho \le 10), \tag{12}$$

where σ is positive for tension loads, Tm is the maximum γ which occurred in any previous cycle, and P is an integer representing the total number of cycles. A regression analysis of the first quarter cycle with $P = 1$ and $\gamma = 0$ indicates that column loading has a minor effect on the shape of the curve. The resulting equation for the first quarter cycle is

$$\frac{M}{M_y} = 0.172 + 1.037 - 0.167\gamma^2 + 0.0084\gamma^3. \tag{13}$$

The derivative of M/My with respect to γ gives the stiffness of the connection which equals bl at zero displacement. The value of b1 is determined from Equation (8) for the first quarter cycle of loading and from (4) for yielded

Figure 5: Fracture patterns of the control specimen.

connections. It is apparent that large displacement levels cause the zero displacement stiffness of these connections to deteriorate rapidly considerably from levels. This could cause lateral responses to vary as predicted by previous data.

(i) Lower column axial compression forces produce smaller hysteresis loops for beam hinges near the beam column interface

(ii) Continued static loading of the connection causes reduction in the size of the hysteresis loop

(iii) An increase in the level of yielding causes a rapid decrease in the stiffness of the connection of zero displacement, as presented in Table 3

5.4. Hysteresis Loop Stimulated in the Excel Spread Sheet

5.4.1. Experimental Data. This is derived from the of hysteresis loops for reinforced-concrete beam column joint connections. Figures 19–22 show the hysteresis loop, displacement, deflection, and displacement for beam column joints under static loading.

This is the hysteresis loop derived from the experiment from the modelling of static implications of joint deformations in RC beam-to-column connections to the overall frame behaviour.

5.5. Finite Element Modelling

5.5.1. Element Type. There are two types of elements used in this analytical work, and they are as follows:

(1) Solid 65-Concrete Element

(2) Link 180-Steel Element

5.5.2. 3D Reinforcement. Solid 65 is used to simulate materials in three dimensions, even without reinforcement steel (rebar). During tension, the material can crack, and in compressing, it can collapse. The substantial

Figure 6: Fracture patterns of Alccofine 5%.

option is available in construction material, for instance, to represent reinforcing behaviour. Reinforced-epoxy composites and geologic materials are examples of further applications again for chemical. Eight nodes with three degrees of freedom each characterize the elements, as do translation in the node x, y, and z directions, as shown in Figure 23. It is possible to declare three different reinforcement requirements.

Steel Link 180 is a reinforcement that can be utilised in a wide range of engineering projects. The component can be conceived of as a truss component, a wire component, a link component, a spring component, and so on, depending on the requirements. The three-dimensional spar element is a three-dimensional uni-axial component with three degrees of freedom at every nodes; translation are in the nodal x, y, and z directions, as shown in Figure 24. Plastic deformation, creep, swelling, and high displacement ability are some factors to be considered.

A discrete mathematical model developed for the linking up of the model is required for the finite element analysis. The model is partitioned into a handful of discrete elements for this purpose, and pressure and stress determined tentatively conclude among these small elements after loading. The mesh density choice is a crucial stage in finite element analysis. Whenever a sufficient number of components are employed in a model, the results converge. Whenever an increase in the mesh size has no effect on the results, this is actually accomplished.

A solution with nonlinearity is the whole applied load to a numerical model that is split into a sequence of plenty of termed load steps in nonlinear analysis. When moving onto next load increment, the structural analysis of the model is updated to reflect unpredictable results associated with building stiffness at the end of the each progressive solution. The modelling modulus is updated using Newton–Raphson equilibria iteration in the ANSYS programme (ANSYS 2010). Under tolerances limitations, Newton–Raphson equilibrium repetitions offer resolution at the conclusion of each load increment. Boundary conditions for the steel and concrete structural system

Figure 7: Fracture patterns of Alccofine 10%.

were based on forces and moments in this work, and the converging tolerances were determined by the ANSYS programme. Figures 25 and 26 show ANSYS finite element modelling and typical ANSYS results. Figure 27 shows deflection ductility of experimental and predicted values of SCC beam column joints.

6. Results and Discussion

According to the testing results, a 10% Alccofine RC beam and column joint provided a considerable boost in the strength of maximum loading condition. The effect on the tensile fracture strengthening of concrete owing to containment by the crimp steel fiber can be attributable to this. When compared to control specimens, Alccofine raised the strength of self-consolidated RC beam column joints with steel fiber by 12.64 percent to 14.65 percent. As compared with the control specimen, the load-bearing capacity of the Alccofine RC composite beams joint improved by 14.65% at the end of the performance.

6.1. Comparison of Experimental Results with FEM Results. Empirical and parameter estimation analysis were used to determine the stress vs. displacement behaviour of all examined beam and column joint specimens. The numerical simulation models' behaviour agrees well with observation and information from the practical experiments. The projected final deflection of finite element model is extremely close to the observed data.

Figure 8: Fracture patterns of Alccofine 15%.

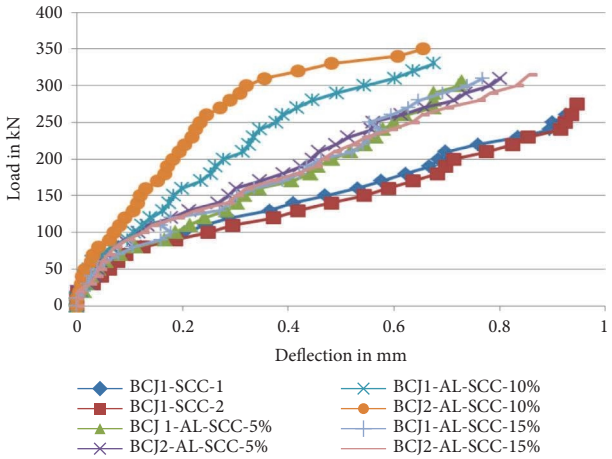

Figure 9: Load vs. deflection behaviour of all tested SCC-BCJ specimens.

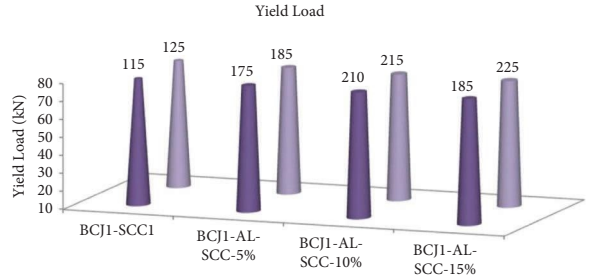

Figure 10: Yield load vs. BCJ specimens.

Table 2: Results at the ultimate level.

Designation for specimen	Yield load (kN)	Critical load (kN)	Yield deflection (mm)	Critical deflection (mm)	Critical stress (MPa)	Critical lateral strain (MPa)
BCJ1-SCC1	115	260	0.480769	0.922	8.666	0.0039
BCJ2-SCC2	125	275	0.478469	0.945	9.166	0.0039
BCJ1-AL-SCC-5%	175	305	0.418852	0.729	10.166	0.0041
BCJ2-AL-SCC-5%	185	310	0.459516	0.77	10.330	0.0042
BCJ1-AL-SCC-10%	210	330	0.439091	0.629	11.000	0.0060
BCJ2-AL-SCC-10%	215	350	0.405429	0.66	11.670	0.0062
BCJ1-AL-SCC-15%	185	310	0.571429	0.88	10.330	0.0081
BCJ2-AL-SCC-15%	225	315	0.525161	0.802	10.500	0.0097

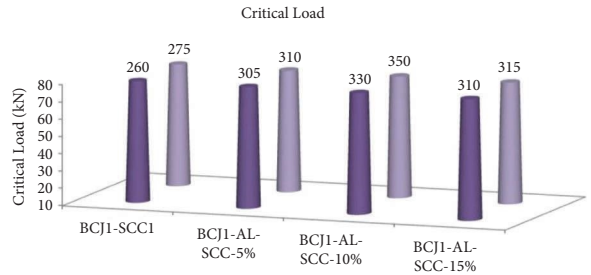

Figure 11: Ultimate load vs. BCJ specimens.

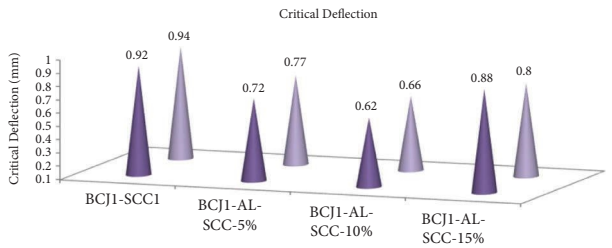

Figure 12: Ultimate deflection vs. BCJ specimens.

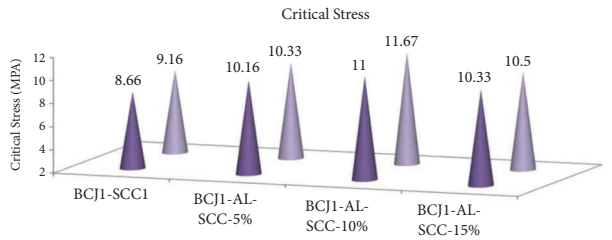

Figure 13: Ultimate stress vs. BCJ specimens.

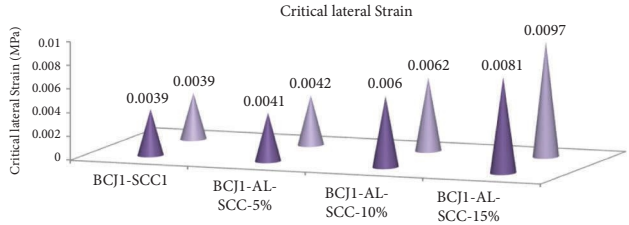

Figure 14: Ultimate lateral micro-strain vs. BCJ specimens.

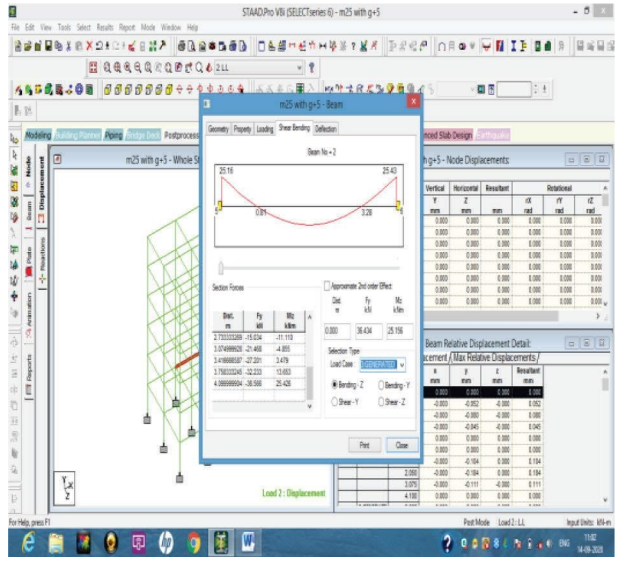

Figure 15: Deflected shapes of $G+5$ in the X and Z direction.

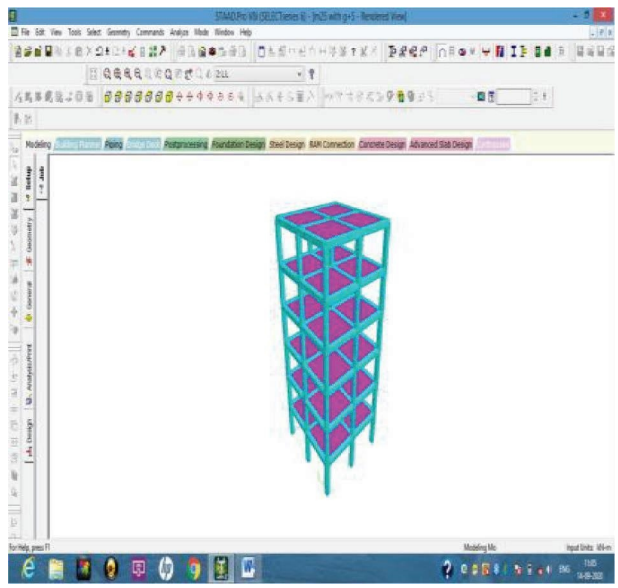

Figure 16: 3D view of $G+5$ RC structures.

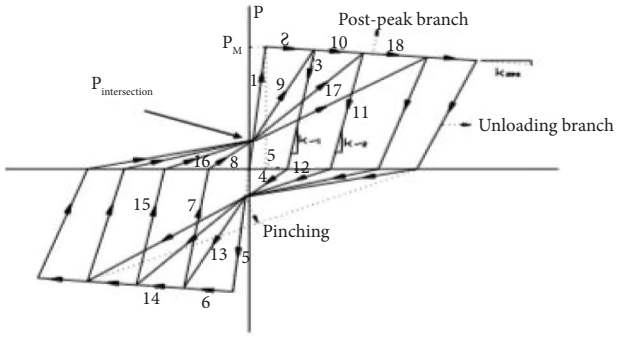

Figure 17: Loop modelling.

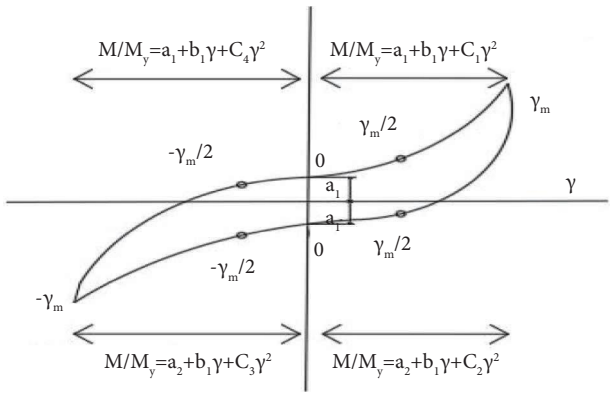

Figure 18: Parabolas in a hysteresis loop.

Table 3: Stiffness at zero displacement.

Displacement level	Stiffness	Uncracked stiffness
0	3.37	100
0 (equation (9))	1.03	30.5
2	0.566	16.8
3	0.458	13.6
5	0.363	10.7
10	0.208	6.1

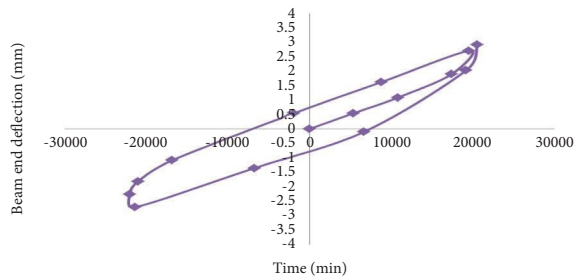

Figure 19: Hysteresis loop for static loading.

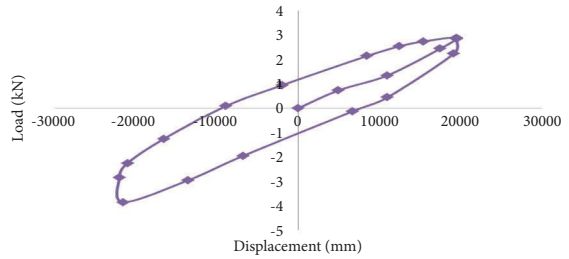

Figure 20: Displacement hysteresis loop for static loading.

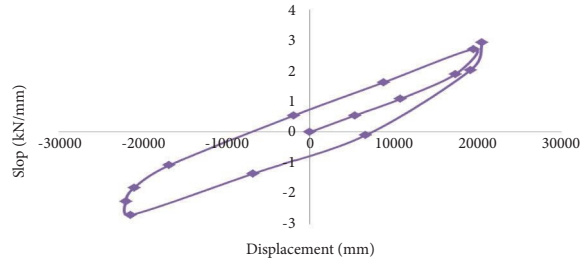

Figure 21: Deflection hysteresis loop for static loading.

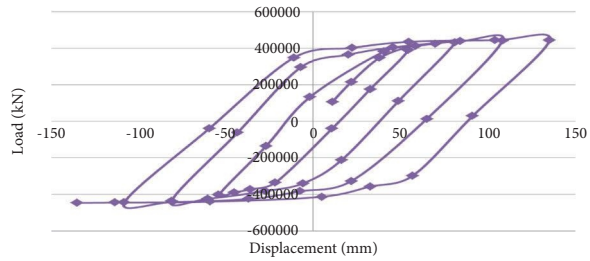

Figure 22: Displacement hysteresis loop for beam column joints.

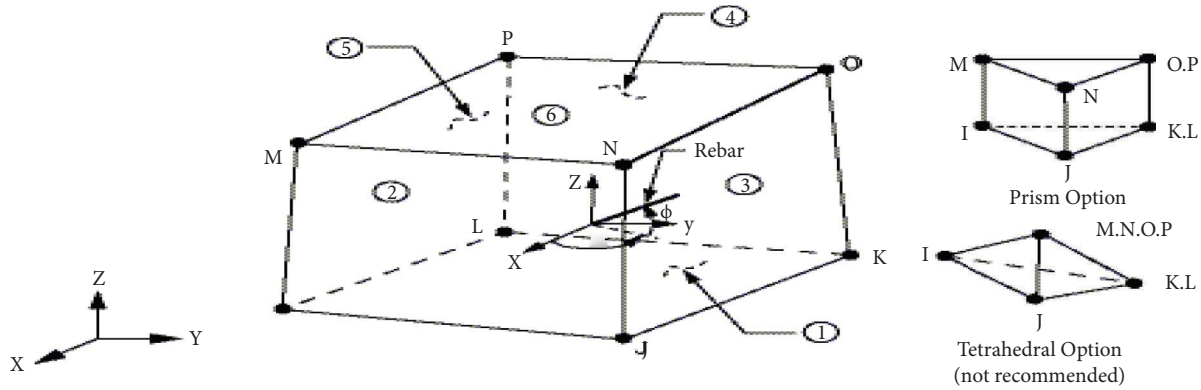

Figure 23: Geometry of element solid 65.

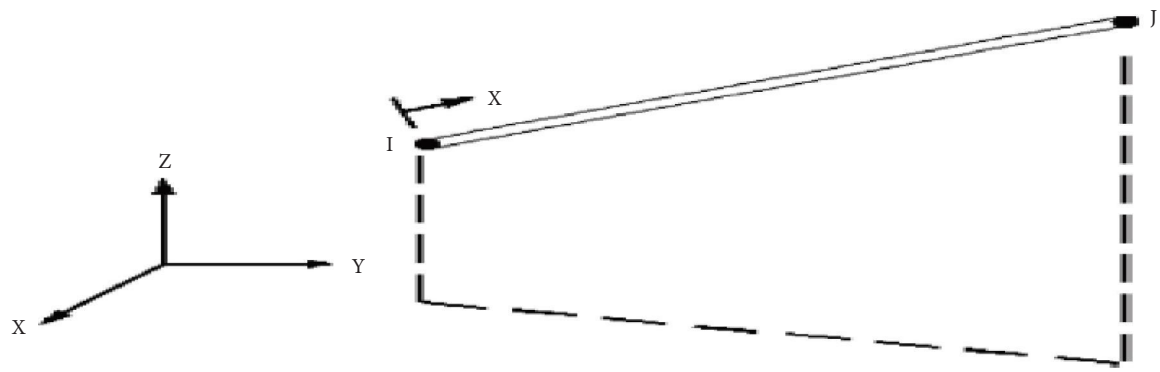

Figure 24: Geometry of element link 180.

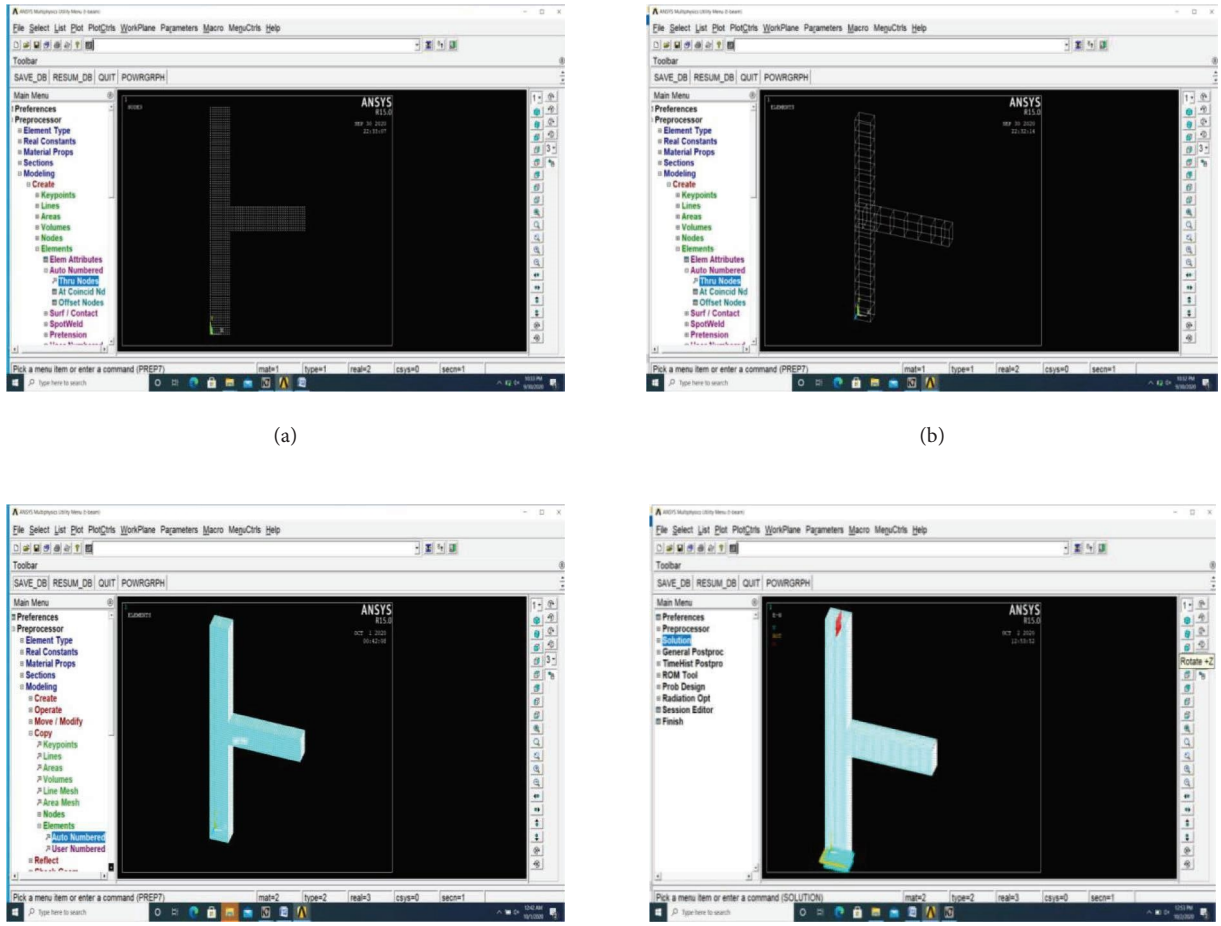

FIGURE 25: ANSYS finite element modelling: (a) node formation, (b) generation of steel element, (c) generation of solid element, and (d) loading condition.

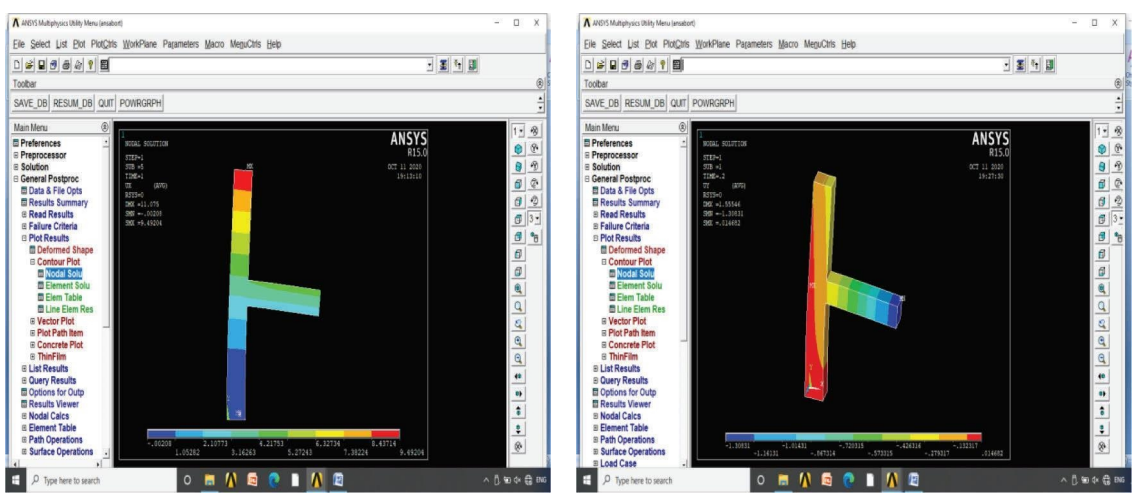

FIGURE 26: Typical ANSYS results: (a) control specimen and (b) SCC with Alccofine-10% specimen.

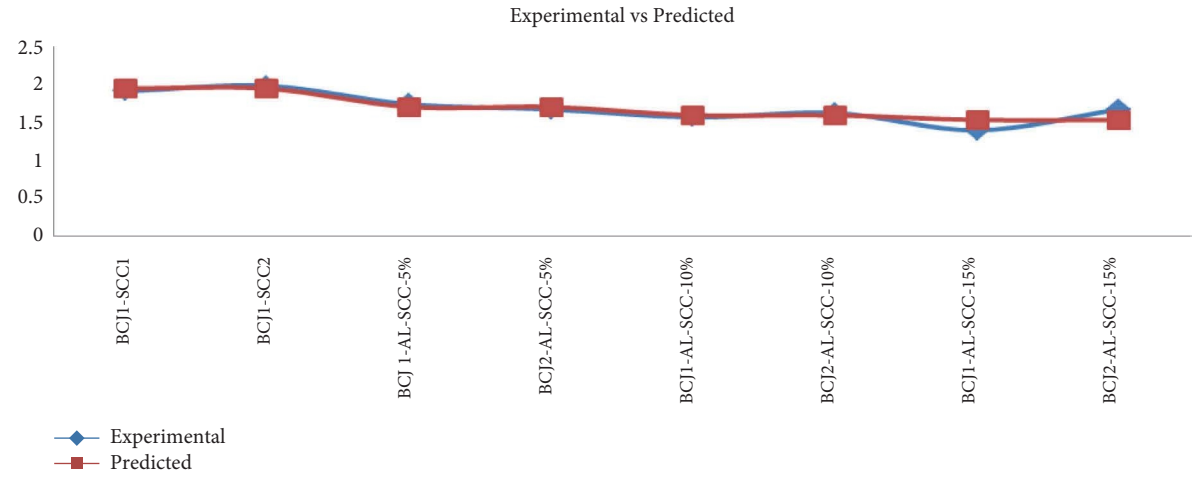

Figure 27: Deflection ductility of experimental and predicted value.

7. Conclusions

This research aims to develop effective self-consolidated concrete beam column joints to enhance according to the test results on self-consolidate RC with Alccofine by cement's partial replacement.

(i) The self-consolidation concrete is done by using Alccofine, superplasticizer, steel fiber, and viscosity modification agent as per EFNARC guidelines

(ii) The present investigation shows that it is possible to achieve self-consolidated concrete with optimum 10% Alccofine

(iii) Strengthening of RC beam column joint with self-consolidation concrete using Alccofine with steel fiber exhibits higher load-carrying capacity and the strengthened self-consolidation RC beam column joint failed in the ductile mode

(iv) The strength increased in the range of 12.64% to 14.65% for self-consolidate RC beam column joint with 10% Alccofine

(v) The nonlinear finite element models give the better performance than the other methods

(vi) The failure mechanism of a self-consolidation RC beam column joints demonstrated quite well by means of ANSYS and also the ultimate deflection anticipated is actually close to the experimental results

Data Availability

The reference articles data used to support the findings of this study are included within this article.

Conflicts of Interest

The authors declare that they have no conflicts of interest.

References

[1] M. SiefaldeenOdaaaMahir, A. HasonbAmjad, and K. Sharbac, "Self-compacting concrete beams reinforced with steel fiber under flexural loads: a ductility index evaluation" Materials," *Today's Office: Proceedings*, vol. 42, no. 5, pp. 2259–2267, 2021.

[2] B. Nambiyanna, M. N. Chandan, and R. Prabhakara, "Flexural performance of exterior steel fiber reinforced self-compacting concrete beam-column joint subjected to reversed cyclic loading," *Journal of Computational and Theoretical Nanoscience*, vol. 17, no. 9, pp. 3934–3939, 2020.

[3] T. Rai and S. V. B. Bibhuti Bhusan Mukharjee, "Beam-column joints made of self-compacting concrete containing recycled coarse aggregates and nano-silica" International," *Journal of Sustainable Materials and Structural Systems*, vol. 4, no. 1, pp. 91–104, 2020.

[4] C. Prithiviraj and J. Saravanan, "Flexural performance of alccofine-based self-compacting concrete reinforced with steel and GFRP bars," *International Transaction Journal of Engineering, Management, & Applied Sciences & Technologies*, vol. 12, no. 8, p. 113, Article ID 12A8U, 2021.

[5] A. Hassan, F. Khairallah, H. Mamdouh, and M. Kamal, "Structural behaviour of self-compacting concrete columns reinforced by steel and glass fibre-reinforced polymer rebars under eccentric loads," *Engineering Structures*, vol. 188, pp. 717–728, 2019.

[6] B. M. Rao and ChavaSrinivas, "Comparison of Structural Behaviour of Beam Column Joints with Conventional Concrete and Self Compacted Concrete," *Journal of emerging technologies and innovative research*, vol. 5, no. 6, 2018.

[7] M. A. Najafgholipour, S. M. Dehghan, A. Dooshabi, and A. Niroomandi, "Finite element analysis of reinforced concrete beam-column connections with governing joint shear failure mode," *Latin American Journal of Solids and Structures*, vol. 14, no. 7, pp. 1200–1225, 2017.

[8] M. Ghasemi, M. R. Ghasemi, and S. R. Mousavi, "Studying the fracture parameters and size effect of steel fiber-reinforced self-compacting concrete," *Construction and Building Materials*, vol. 201, pp. 447–460, 2019.

[9] B. Venkatesan, R. Ilangovan, P. Jayabalan, N. Mahendran, and N. Sakthieswaran, "Finite element analysis (FEA) for the beam-column joint subjected to cyclic loading was performed using ANSYS," *Circuits and Systems*, vol. 7, no. 8, pp. 1581–1597, 2016.

[10] H. Shirazi and M. Esfahani, "Effect of self-consolidating concrete on beam-column exterior," *Joints" Amirkabir Journal of Science & Research (Civil & Environmental Engineering)*, vol. 45, no. 1, pp. 25–27, 2013.

[11] A. M. Said and M. L. Nehdi, "Behaviour of beam-column joints cast using selfconsolidating concrete under reversed cyclic loading," in *Proceedings of the 13th World Conference on Earthquake Engineering Vancouver*, Vancover, Canada, August 2004.

[12] J. Hegger, AlaaSherif, and W. Roeser, "Nonlinear finite element analysis of reinforced concrete beam-column connections," *ACI Structural Journal*, vol. 101, p. 5, 2004.

[13] M. SoleymaniAshtiani, R. P. Dhakal, and A. N. Scott, "Using high-strength self-compacting concrete in reinforced concrete beam-column joints," in *Proceedings of the Conference New Zealand Society for Earthquake Engineering (NZSEE2013)*, Wellington, New Zealand, April 2013.

[14] L. V. Meesaraganda, P. Saha, and A. I. Laskar, "Behaviour of self-compacting reinforced concrete beams strengthened with hybrid fiber under Static and cyclic loading," *International Journal of Civil Engineering*, vol. 16, no. 2, pp. 169–178, 2018.

[15] B. V. Kavyateja, J. Guru Jawahar, and C. Sashidhar, "Effectiveness of alccofine and fly ash on mechanical properties of ternary blended self compacting concrete," *Materials Today Proceedings*, vol. 33, no. 1, pp. 73–79, 2020.

[16] C. Prithiviraj and J. Saravanan, "Influence of W/B ratio and chemical admixture on fresh and hardened properties of self compacting concrete using alccofine," *Journal of Xidian University*, vol. 14, no. 5, 2020.

[17] B. Sagar and M. V. N. Sivakumar, "An experimental and analytical study on alccofine based high strength concrete," *International Journal of Engineering*, vol. 33, no. 4, pp. 530–538, 2020.